https://doi.org/10.1016/j.engstruct.2021.111930

Full-Scale Experimental and Numerical Investigation on the Ductility, Plastic Redistribution, and Redundancy of Deteriorated Concrete Bridges

Xiaoming Wang[1], Xiangyuan Mao[2], Dan M. Frangopol[3], You Dong[4,*], Huan Wang[5], Pei Tao[6], Zezhong Qi[7], and Shengpeng Tang[8]

[1] *Associate Professor, Key Laboratory of Transport Industry of Bridge Detection Reinforcement Technology (Chang'an University), Chang'an University, Xi'an, 710064, Shaanxi Province, China. E-mail: wxm@chd.edu.cn*

[2] *Graduate Student, Key Laboratory for Bridge and Tunnel of Shaanxi Province, Chang'an University, Xi'an 710064, Shaanxi Province, China. E-mail: mxy_chd@163.com*

[3] *Professor and the Fazlur R. Khan Endowed Chair of Structural Engineering and Architecture, Dept. of Civil and Environmental Engineering, ATLSS Engineering Research Center, Lehigh University, 117 ATLSS Dr., Bethlehem, PA 18015-4729, E-mail: dan.frangopol@lehigh.edu*

[4,*] *Assistant Professor, Dept. of Civil and Environmental Engineering, Hong Kong Polytechnic University, Hong Kong, China (corresponding author). E-mail: you.dong@polyu.edu.hk*

[5] *Graduate Student, Key Laboratory for Bridge and Tunnel of Shaanxi Province, Chang'an University, Xi'an 710064, Shaanxi Province, China. E-mail: wh_chd@163.com*

[6] *Graduate Student, Key Laboratory for Bridge and Tunnel of Shaanxi Province, Chang'an University, Xi'an 710064, Shaanxi Province, China. E-mail: tp_chd@qq.com*

[7] *Graduate Student, Key Laboratory for Bridge and Tunnel of Shaanxi Province, Chang'an University, Xi'an 710064, Shaanxi Province, China. E-mail: qzz_chd@163.com*

[8] *Graduate Student, Key Laboratory for Bridge and Tunnel of Shaanxi Province, Chang'an University, Xi'an 710064, Shaanxi Province, China. E-mail: tsp_chd@163.com*

ABSTRACT:

Due to structural degradation, the performance of concrete bridges may degrade with time and result in catastrophic consequences. A novel approach is developed for evaluating the time-variant reliability of multi-girder concrete bridges considering the effects of the load-carrying mechanism and redundancy. By considering three failure modes at both the component and system levels, a new performance indicator is proposed for quantitatively evaluating the load elastic distribution and plastic redistribution among multiple girders. The adverse effects of material deterioration on the structural capacity, ductility, redundancy, load-carrying capacity, and failure mechanism are also investigated and incorporated into the analytical procedure, in which an incremental nonlinear finite element analysis of a 3D fiber beam element is used. Furthermore, full-scale destructive failure tests of two in situ deteriorated bridges, a reinforced concrete (RC) and a prestressed RC (PRC) T-girder bridge, are conducted to evaluate the accuracy of the proposed approach. The feasibility and satisfactory performance of the proposed framework are evaluated using these two real-world bridges. The results demonstrate that the load-carrying mechanism and redundancy significantly affect the structural ultimate load-carrying capacity and time-variant reliability of deteriorating structures.

Keywords:

Multi-girder bridge
Load-carrying mechanism
Ductility
Plastic redistribution
Time-variant system reliability and redundancy

Nomenclature

SGFM	single-girder failure mode.	E_{s0} f_{y0} f_{u0} ε_{sy0} ε_{su0}	elastic modulus, yield strength, ultimate strength, yield strain, and ultimate strain of uncorroded steel bar, respectively.
MGFM-ED	multi-girders failure mode under elastic distribution of load.		
MGFM-PR	multi-girders failure mode by considering plastic redistribution of load.	σ_{pc} ε_{pc}	stress and strain of corroded prestressed tendons, respectively.
FEM	finite element analysis.	η_p $\eta_{p,cr}$	corrosion rate and threshold value of corrosion extent of corroded prestressed tendons, respectively.
ULS	ultimate limit state.		
P_c P_e P_u	the ultimate wheel load under the worst-case of vehicle loading for SGFM, MGFM-ED and MGFM-PR, respectively.	E_{pc} f_{puc} ε_{puc}	elastic modulus, ultimate strength, and ultimate strain of corroded prestressed tendons, respectively.
m	load transverse distribution coefficient.	E_{p0} f_{pu0} ε_{pu0}	elastic modulus, ultimate strength and ultimate strain of uncorroded prestressed tendon, respectively.
L_c LF_e LF_u	the ultimate vehicle load for SGFM, MGFM-ED, and MGFM-PR, respectively.	μ_c	ductility coefficient (at component level).
		$MCRs$	moment-curvature relationships
σ_{sc} ε_{sc}	stress and strain of corroded steel bars.	φ_u φ_y	section curvatures at failure point and yielding point of MCRs curve.
η_s $\eta_{s,cr}$	corrosion rate and threshold value of corrosion extent of corroded steel bars.	R_u	system redundancy.
f_{yc} f_{uc} ε_{syc} ε_{shc} ε_{suc}	yield strength, ultimate strength, yield strain, hardening strain, and ultimate strain of corroded steel bars, respectively.	PI_c $PI_{s,u}$	the probability contributions of SGFM and MGFM-PR to system failure.

1 Introduction

Structural engineering is undergoing a profound change toward a life-cycle-oriented design philosophy to satisfy the continuously increasing demands in response to economic, environmental, social, and political requirements [1-3]. During their service lives, reinforced concrete (RC) and prestressed RC (PRC) bridges may exhibit severe damage due to variety of environmental and mechanical stressors [4-6]. Damage may impair structural reliability and requires increasing inspection and maintenance costs. During the past four decades, accidents frequently occurred, such as the collapses of the Mianus River bridge in 1983, the SR1014 bridge over I-70 in 2005, the I-35W Mississippi River bridge in 2007 [7], the I-5 Skagit River bridge in 2013 [8], the Morandi bridge in 2018 [9, 10] and the Wuxi single-column bridge in 2019. These have aroused concern regarding the performance assessment and management of aging bridges. Therefore, studies on the reliability assessment of deteriorated bridges at both the component and system levels are of vital importance for maintaining sufficient reliability levels of both serviceability and ultimate performance [11, 12].

To address these issues, many studies have been conducted to assess the performance of deteriorated structural components. For instance, Melchers [13] conducted a reliability assessment by considering the degradation of the structural performance, Val [14] assessed the component performance of the critical sections, and Hamdia [15] presented a fuzzy-based assessment model for estimating the importance of structural assessment criteria for RC structures. These studies focused on the strength degradation of load-carrying components that is caused by material deterioration. The ultimate limit state of the most vulnerable component was evaluated after determining the internal force distribution among the load-carrying components. In these studies, only the most vulnerable component was investigated in detail by considering the ultimate limit state.

Afterwards, studies on the system-level performance were conducted based on the series-parallel model. For instance, Frangopol [16] assumed that failure of any two or three adjacent girders can cause failure of the superstructure within a multi-girder bridge, and Li [17] assumed the failure of three adjacent I-shaped steel girders as the failure criterion of the structure system. These studies assessed the system-level performance by using failure probabilities of multiple

girders linked in a series-parallel system, which directly reflect the importance of each component to the system. However, the plastic redistribution of the internal force was not always considered, and the number of parallel girders was determined via empirical estimation, resulting in an insufficient basis for the establishment of system failure criteria [18-20]. To address these issues, structural system failure analysis using the finite element method (FEM) was used in many studies to simulate the failure process of the structure and to analyze the ultimate load-carrying capacity of the corresponding bridge system [21, 22]. To consider the uncertainties within the analysis process, the FEM should be conducted repeatedly, which is relatively computationally expensive and cannot be rapidly incorporated into the reliability analysis process. Meanwhile, the accuracy of the FEM should be evaluated. Thus, an efficient and accurate model should be developed for the time-variant performance assessment of deteriorated structures by considering the plastic redistribution. Recently, many destructive failure tests have been designed and conducted to evaluate the failure criterion [23], but most are component-level tests. In this paper, a new system assessment method is proposed for multi-girder bridges that uses full-scale destructive failure tests and a precise finite element modeling method.

The system redundancy is another essential indicator for system-level structural performance evaluation, which is defined as the ability of the bridge system to redistribute the applied load after reaching the ultimate load-carrying capacity of the most vulnerable component within the system [16, 24-34]. Typically, the failure of a single component would not cause the failure of the whole structure [35, 36]. Research on system redundancy has been extensively conducted in the recent decades. For instance, Wen *et al.* [37] investigated the redundancy of special moment resisting frames and dual systems under seismic excitations, Kim *et al*. [38] evaluated the redundancy of a steel box-girder bridge by using a nonlinear finite element model, Biondini *et al*. [39] developed a probabilistic procedure for time-variant redundancy assessment of concrete structures that are exposed to corrosion, and Tu *et al*. [40] considered the relevant adverse effects that are induced by reinforcement corrosion at various levels when assessing the redundancy of a multi-girder PRC bridge. In these studies, the effects of material deterioration on the degradation of the girder's resistance and the system redundancy were assessed. However, these studies were based on the assumption that the system-level load-carrying mechanism is unchanged. Considering the deterioration, the load-carrying mechanism of the system may no longer follow the design scenario.

Another important aspect that should be considered within the redundancy analysis is the contribution of the transverse connection, which was often ignored in the previous studies. Considering deteriorated multi-girder bridges as an example, the performance of the transverse connection has a significant influence on the system-level load-carrying mechanism [41, 42]. If the transverse connection fails, the probability of a system failure caused by a single-girder failure mode would significantly increase; When the transverse connection is intact, a bridge system will fail in a typical multi-girder failure mode. Meanwhile, the change of the load-carrying mechanism that is caused by material deterioration and damage accumulation is a random process. Studies should be conducted to assess the effects of the time-variant system-level load-carrying mechanism and its randomness on the structural reliability and redundancy. In this paper, the coupling effect of the time-variant redundancy and the load-carrying mechanism on the system-level performance is considered.

In this study, a novel assessment approach is developed for evaluating the time-variant system reliability and redundancy of multi-girder bridges by considering the effects of the load-carrying mechanism, transverse connection, and plastic redistribution. This aspect acts as one contribution of this study. In addition, based on the analysis of failure modes at both the component and system levels, a new indicator is proposed in Section 2 for quantitatively evaluating the performance in terms of the load elastic distribution and plastic redistribution among multiple girders. In this way, a system-level redundancy indicator is derived by considering more aspects, which acts as another contribution of this paper. The adverse effects of material deterioration on the structural capacity, ductility, redundancy and load-carrying mechanism are investigated in Section 3. A computational framework for the system reliability is presented, in which the effects of the time-variant load-carrying mechanism and redundancy on the bridge system are considered. An analytical procedure with detailed modeling techniques is established in Section 4 for implementing the proposed assessment framework, in which an incremental nonlinear finite element analysis of a 3D fiber beam element that utilizes OpenSees is employed. Two full-scale destructive tests of in situ deteriorated bridges are conducted to evaluate the accuracy of the proposed analytical procedure. The feasibility and satisfactory performance of the proposed framework and procedure are evaluated using RC and PRC T-girder bridges. The results demonstrate that the time-variant load-

carrying mechanism and redundancy significantly affect the structural ultimate load-carrying capacity and the reliability of deteriorated structures.

2 Flexural Failure Modes of Multi-Girder Bridges

Multi-girder bridges have been widely used in practical applications due to their advantages in terms of construction and mechanical behavior [43, 44]. Considering the spatial integrity of the structure, when a live load is applied to the bridge, the girders work together [45]. A reliability assessment of multi-girder bridges must consider the relevant failure mode physically. As a basic structural form, the failure mode of a single girder has been widely investigated. However, multi-girder bridges are composed of multiple girders, which are connected into a spatial structure using transverse connections, and the failure mode at the system level considering transverse connection still must be investigated.

2.1 Effect of the transverse connection on the failure mode of multi-girder bridges

As presented in Fig. 1, for multi-girder bridges, the main girder is the load-carrying component, and the transverse connection is the transverse load-transferring component. Therefore, multiple girders interact to carry loading via the transverse connection. This interaction load-carrying mechanism and the failure mode of system are affected by many factors. Material deterioration would lead to not only the decrease of girders resistance but also performance degradation of the whole structure, resulting in changes in the interaction load-carrying mechanism and the structural failure mode. In this paper, the relevant parameters are considered within the performance assessment of the deteriorated structures.

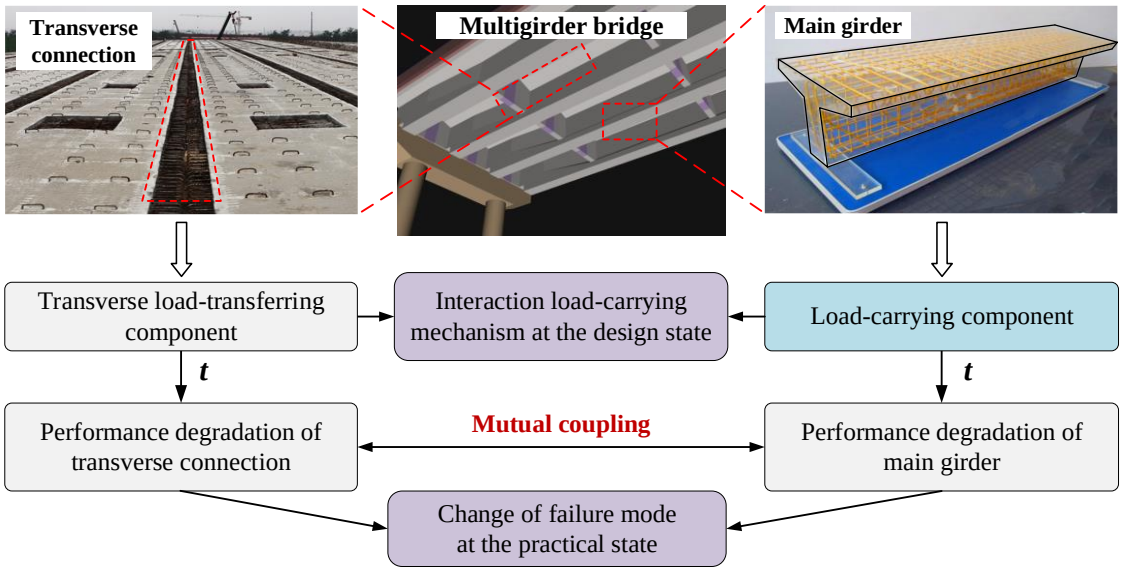

Fig. 1. Load-carrying mechanism of a multi-girder bridge.

This study focuses on flexural failure under the worst-case scenario of vehicle loading, which is the most likely failure scenario for multi-girder bridges. If any main girder within the system fails due to exceeding material strength or the maximum vertical deflection exceeds l/100 of the bridge span [46-48], the multi-girder bridge system is regarded as having reached the ultimate limit state (ULS) and fails.

2.2 Flexural failure modes

In this paper, based on an investigation of real-world accidents of multi-girder bridges, two main forms of failure modes are considered: single-girder failure mode (SGFM) and multi-girder failure mode (MGFM). Based on the bridge design specifications [46, 47], the multi-girder failure modes can be divided into multi-girder failure mode under the elastic distribution of the load (MGFM-ED) and multi-girder failure mode by considering the plastic redistribution of the load (MGFM-PR).

2.2.1 Single-girder failure mode

As shown in Fig. 2 (a), if the transverse connection fails, the load-transferring route among adjacent girders is cut off, thereby resulting in the loss of the interaction load-carrying mechanism among multiple girders. In this case, any single-girder within the system that exceeds ULS will cause a structural failure, which can be defined as a SGFM.

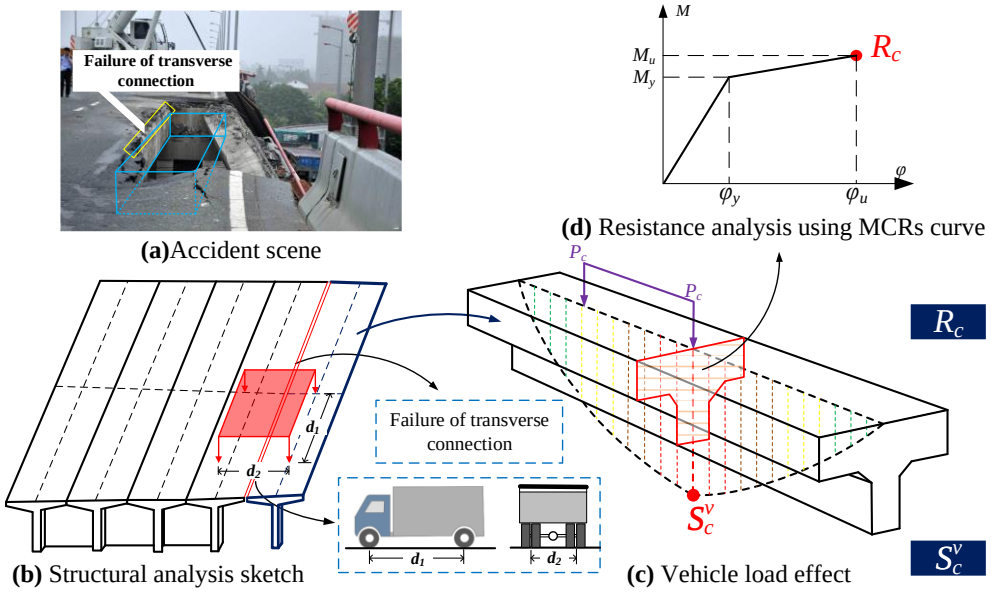

Fig. 2. Single-girder failure mode.

As illustrated in Fig. 2 (b) and (c), the ultimate vehicle load for SGFM L_c can be expressed as

$$L_c = 2P_c \tag{1}$$

where P_c is the ultimate wheel load under the worst-case scenario of vehicle loading for SGFM.

The corresponding limit state function of SGFM Z_c is

$$Z_c = R_c - S_c^G - S_c^V \tag{2}$$

where R_c is moment resistance of the single girder for SGFM, which is equal to M_u of the MCR curve, as presented in Fig. 2 (d); S_c^G is the bending moment associated with the dead load effect on the single-girder; and S_c^V is the bending moment from the vehicle load on the single girder for SGFM.

2.2.2 Multi-girder failure mode under the elastic distribution of the load

As illustrated in Fig. 3 (b), when the transverse connection is intact, multiple girders interact to carry the load, and the vehicle load is distributed according to the component stiffness within the initial elastic stage. Once the most vulnerable girder within a bridge has reached its ULS, the whole bridge can be regarded as failed, which is defined as a MGFM-ED [46, 47].

As illustrated in Fig. 3 (b) and (c), the ultimate vehicle load for MGFM-ED LF_e can be expressed as

$$LF_e = n \cdot P_e \tag{3}$$

where n and P_e are the number of the wheel load points and the ultimate wheel load under the worst-case scenario of vehicle loading for MGFM-ED, respectively.

Herein, a new indicator, namely, the effective number of girders N_e is proposed for quantitatively evaluating the ability of the system to distribute a vehicle load for MGFM-ED. This number is defined as

$$N_e = LF_e / L_c \tag{4}$$

Based on the design specifications [46], LF_e can also be computed as

$$LF_e = L_c / m \tag{5}$$

where m is the load transverse distribution coefficient [46] representing the proportion of the load that is carried by the most vulnerable girder within a bridge in the elastic range. From Eq. (4) and (5), it follows that $N_e = 1/m$.

The corresponding limit-state function of MGFM-ED, denoted as $Z_{s,e}$, is

$$Z_{s,e} = R_{s,e} - S_s^G - S_{s,e}^V \tag{6}$$

where $R_{s,e}$ is the moment resistance of the bridge system for MGFM-ED; S_s^G is the dead-load bending effect of the bridge system; and $S_{s,\mathrm{e}}^V$ is the vehicle-load bending effect for MGFM-ED, which is equal to $\sum M_i^v$, where M_i^v is the vehicle load effect on each girder.

MGFM-ED approximately reflects the ULS of the bridge system, as it combines the load distribution that is based on the initial elastic analysis with the ultimate and plastic load-carrying capacities of the most vulnerable components. This could result in a contradiction between the elastic analysis at the system level and the ultimate load-carrying capacity design at the structural component level. Only the elastic distribution of the internal forces is considered within the analytical method, while the plastic redistribution is not. As a result, this method fails to capture

the critical state of the ultimate load-carrying capacity of the whole structural system, and the real ultimate load-carrying capacity at the system level is not considered, namely, only an approximate value that is based on the elastic distribution of the internal forces is provided.

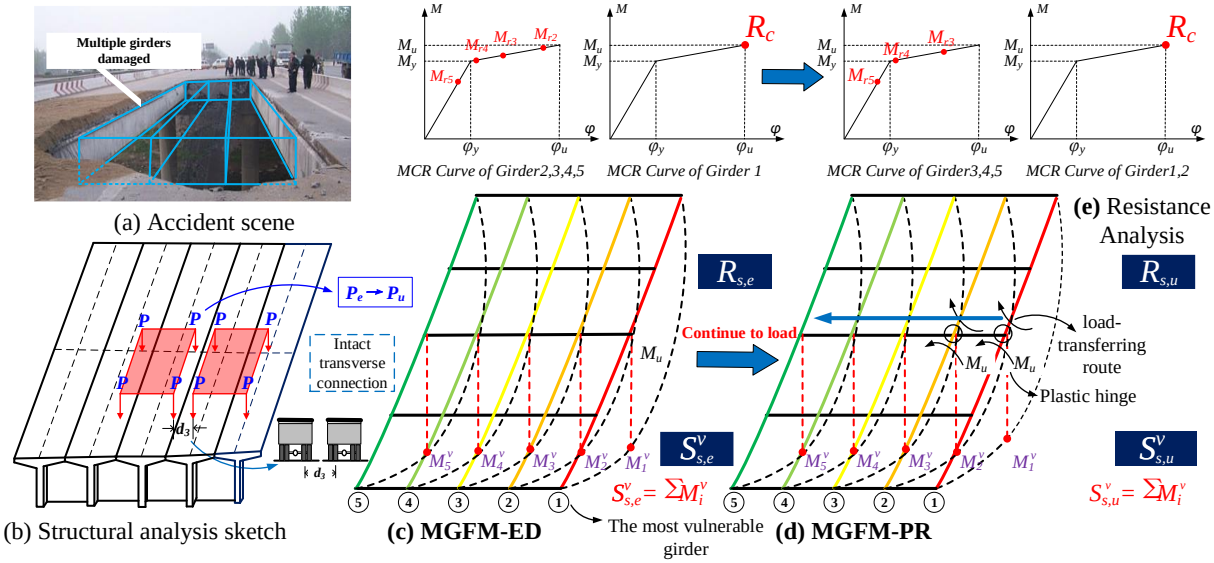

Fig. 3. Multi-girder failure mode.

2.2.3 Multi-girder failure mode by considering the plastic redistribution of the load

As illustrated in Fig. 3 (b), when the transverse connection is intact, multiple girders work together to carry the load. With the increase of the external vehicle load, the distribution of the load among the girders gradually changes from an elastic distribution that is based on the stiffness to a plastic redistribution by considering the ductility. Once the system exceeds the ULS, the system fails. This is defined as a MGFM-PR.

As shown in Fig. 3 (d), the flexural failure could be regarded as a ductile failure in most cases [49], however, concrete components with serious steel corrosion can exhibit the brittle failure. By considering the ductility of the main girder, the load distribution mechanism may change before the most vulnerable girder reaches the plastic hinge rotation limit state. In this scenario, the adjacent girders would be subjected to the increasing external load that is released by the failure component. The ultimate vehicle load for MGFM-PR LF_u is the ultimate load-carrying capacity of the bridge system, which could exceed the ultimate vehicle load for MGFM-ED LF_e; thus, the contradiction between the elastic analysis at the system level and the ultimate load-carrying capacity design at the component level that was described previously is eliminated.

As presented in Fig. 3 (b) and (d), the ultimate vehicle load for MGFM-PR is

$$LF_u = n \cdot P_u \tag{7}$$

where n and P_u are the number of the wheel load points and the ultimate wheel load under the worst-case scenario of vehicle loading for MGFM-PR, respectively.

An indicator, namely, the effective number of girders N_u, is proposed for quantitatively evaluating the ability of the system to distribute vehicle load for MGFM-PR. This indicator can be expressed as

$$N_u = LF_u / L_c \tag{8}$$

$N_e \le N_u \le Num$, in which Num is the number of girders within the bridge. Based on this, an indicator λ is defined for evaluating the plastic redistribution ability of the bridge system as follows:

$$\lambda = N_u / N_e \tag{9}$$

For a multi-girder system, once the topological configuration of the system has been determined, the ductility of the component is the main factor that affects the plastic redistribution ability λ. The corresponding limit state function of MGFM-PR $Z_{s,u}$ is

$$Z_{s,u} = R_{s,u} - S_s^G - S_{s,u}^V \tag{10}$$

where $R_{s,u}$ is the moment resistance of the bridge system for MGFM-PR and $S_{s,u}^V$ is the vehicle-load bending effect for MGFM-ED, which is equal to $\sum M_i^v$, where M_i^v is the vehicle-load bending effect on each girder.

3 Time-Variant System Performance

3.1 Time-variant material behavior

3.1.1 Time-variant material behavior of the reinforcement

As bridges are typically directly exposed to the environment, their performances decrease over time. For RC and PRC bridges, corrosion of reinforcement is one of the primary sources of deterioration of the structures [50]. There are various categories of steel corrosion, among which

the most common are the carbonization-induced uniform corrosion and pitting corrosion that are caused by chloride erosion. Corrosion will lead to loss of the stress section and reduction of the ultimate/yield strength and the stress concentration, which will further reduce the structural resistances of individual components and of the whole system [40].

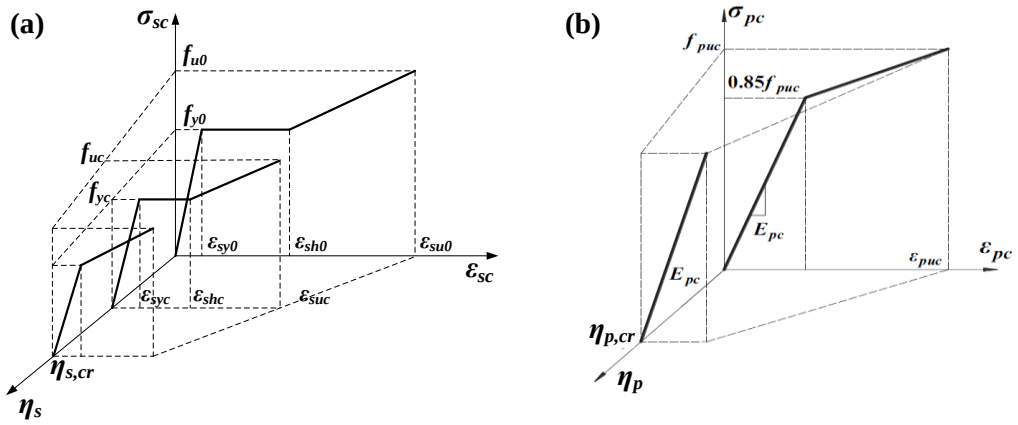

Fig. 4. Constitutive model of corroded (a) steel bars and (b) prestressed tendons under tension

In addition to the adverse effects described previously, corrosion can reduce the ductility of steel bars, which is manifested by the shortening of the yield plateau or even its disappearance [51]. If the value of the corrosion rate η_s is less than the threshold value of the corrosion extent $\eta_{s,cr}$, the yield plateau becomes shorter with the increase of the corrosion; if η_s exceeds $\eta_{s,cr}$, the hardening strain ε_{shc} coincides with the yield strain ε_{syc}, and the yield plateau disappears. As the redistribution of internal forces often occurs within the yield plateau stage, additional studies should be conducted to assess the relevant influences on the structural behavior at both the component and system levels.

Based on tensile tests, Zhang *et al*. [51] concluded that the value of the elastic modulus E_{sc} of a corroded steel bar remained nearly constant; however, the yield strength f_{yc}, the ultimate strength f_{uc} and the ultimate strain ε_{suc} deteriorated as the corrosion propagated. The constitutive relationship of corroded steel bars that are subjected to tension can be described as illustrated in Fig. 4 (a), as follows

$$\sigma_{sc}=\begin{cases} E_{s0}\varepsilon_{sc} & \text{if } \varepsilon_{sc}\le f_{yc}/E_{s0} \\ f_{yc} & \text{if } f_{yc}/E_{s0}<\varepsilon_{sc}\le\varepsilon_{shc} \\ f_{yc}+\left(\dfrac{\varepsilon_{sc}-\varepsilon_{shc}}{\varepsilon_{suc}-\varepsilon_{shc}}\right)\cdot(f_{uc}-f_{yc}) & \text{if } \varepsilon_{sc}>\varepsilon_{shc} \end{cases} \tag{11}$$

where σ_{sc} and ε_{sc} are the tension stress and strain, respectively, of the corroded steel bars.

The variation of ε_{shc} can be expressed as

$$\varepsilon_{shc}=\begin{cases} \dfrac{f_{yc}}{E_{s0}}+\left(\varepsilon_{sh0}-\dfrac{f_{y0}}{E_{s0}}\right)\cdot\left(1-\dfrac{\eta_s}{\eta_{s,cr}}\right) & \text{if } \eta_s\le\eta_{s,cr} \\ \varepsilon_{syc}=\dfrac{f_{yc}}{E_{s0}} & \text{if } \eta_s>\eta_{s,cr} \end{cases} \tag{12}$$

where E_{s0}, f_{y0} and ε_{sh0} are the elastic modulus, yield strength and hardening strain, respectively, of the uncorroded steel bars. The values of the characteristic parameters are summarized in Table 1.

Table 1. Characteristic parameter values [51].

f_{yc}, f_{uc}	ε_{shc}	ε_{suc}	$\eta_{s,cr}$	Applicable condition
$f_{yc}=\frac{1-1.049\eta_s}{1-\eta_s}f_{y0}$ $f_{uc}=\frac{1-1.119\eta_s}{1-\eta_s}f_{u0}$	Calculated via Eq. (12)	$\varepsilon_{suc}=e^{-2.501\eta_s}\varepsilon_{su0}$	Deformed: 20% Plain: 10%	Practical engineering: $\eta_s\le 80\%$

The model in Fig. 4 (a) is suitable for steel bars and pretensioned tendons, which are in direct contact with concrete. If prestressed tendons are installed suitably, corrosion is rare. In this paper, to illustrate and quantify the potential effects of corrosion, the effects of the corrosion of prestressed tendons are considered.

Experimental studies have shown that with the increase of corrosion, the ultimate tensile strain ε_{puc} and ultimate stress f_{puc} of the prestressed tendons significantly decreased [52]. The hardening portion within the constitutive model also decreases with the increase of corrosion, which could cause the behavior of the prestressed tendons to change from bilinear elastic to brittle elastic behavior [53].

Define 0.85 f_{puc} as the prestressed tendon nominal yield tension stress f_{pyc}, and the evolution of the constitutive relationship of corroded prestressed tendons that are subjected to tension can be described by Eq. (13) and (14) [53], as presented in Fig. 4 (b).

For $\eta_p \le \eta_{p,cr}$,

$$\sigma_{pc} = \begin{cases} E_{pc}\varepsilon_{pc}, & \text{if } \varepsilon_{pc} \le \dfrac{0.85 f_{puc}}{E_{pc}} \\ 0.85 f_{puc} + \left(\varepsilon_{pc} - \dfrac{0.85 f_{puc}}{E_{pc}}\right) \cdot \left(\dfrac{0.15 f_{puc}}{\varepsilon_{puc} - \dfrac{0.85 f_{puc}}{E_{pc}}}\right), & \text{if } \dfrac{0.85 f_{puc}}{E_{pc}} < \varepsilon_{pc} \le \varepsilon_{puc} \end{cases} \tag{13}$$

For $\eta_p > \eta_{p,cr}$,

$$\sigma_{pc} = E_{pc}\varepsilon_{pc} \tag{14}$$

where σ_{pc} and ε_{pc} are the tension stress and strain, respectively; $\eta_{p,cr}$ is the threshold value of the corrosion extent; and E_{pc}, ε_{puc} and f_{puc} are the elastic modulus, ultimate tension strain, and ultimate tension stress, respectively, of the corroded prestressed tendons, which can be computed as

$$E_{pc} = \left(1 - 0.848\eta_p\right) E_{p0} \tag{15}$$

$$f_{puc} = \frac{1 - 2.683\eta_p}{1 - \eta_p} f_{pu0} \tag{16}$$

$$\varepsilon_{puc} = \left(1 - 9.387\eta_p\right) \varepsilon_{pu0} \tag{17}$$

where E_{p0}, ε_{pu0} and f_{pu0} are the elastic modulus, ultimate tension strain, and stress, respectively, of the uncorroded prestressed tendons.

3.1.2 Time-variant material behaviour of the concrete

Though the corrosion of reinforcements is the principal pathological manifestation in reinforced concrete structures [54], the effect of concrete degradation on the structural durability should also be considered. Many studies have been conducted to established a model that accounts realistically for concrete mechanical degradation with time. For instance, Leonel [55] presented a numerical

nonlinear formulation, in which the physical nonlinearity of concrete is described by Mazars damage model. In this paper, the performance degradation formulation proposed by Zhang [56] is adopted, which is based on the long-term exposure test data and the measured results of old bridges. The diachronic model of concrete strength is described as

$$m_c(t) = \eta(t) m_{c0} \tag{18}$$

$$\sigma_c(t) = \zeta(t) \sigma_{c0} \tag{19}$$

where, m_{c0} and σ_{c0} are the average value and standard deviation of concrete 28d strength, and

$$\eta(t) = 1.3781 \exp[-0.0187(\ln t - 1.7282)^2] \tag{20}$$

$$\zeta(t) = 0.0347t + 0.9772 \tag{21}$$

3.1.3 Spatial variability associated with the material corrosion

Corrosion of steel reinforcement is spatially distributed over RC structures due to several factors (e.g., different environmental exposures, concrete cover, concrete quality). It is important to take the effect of spatial variability on the reliability analysis and prediction of the remaining service life of RC structures [57]. However, as in practice there exists difficulty in quantifying the area of the rebars in the concrete, it is not easy to obtain the relevant parameters for spatial variability modeling [58]. Recently, Akiyama and Frangopol and Lim et al. [59, 60] have used the X-ray and digital image processing techniques to study and quantify the spatial variability in the steel weight losses along the corroded bars inside RC members, which provides an effective simulation method for spatial variability. Given more information, in this paper, the spatial variability information can be incorporated within the developed analytical framework to evaluate the time-dependent system reliability and redundancy.

3.2 Time-variant ductility of the structural components

Material deterioration leads to the deterioration not only of the component resistance but also of the component ductility. The ductility is the ability of a material, section, component, or system to sustain plastic deformation without significant reduction of its strength [61]. The flexural deformation of structural components is associated with their curvature. For example, the curvature of an RC component depends on the tensile strain of the reinforcement steel and the compressive

strain of the concrete. As concrete is a material with limited ductility compared with steel, RC components realize ductility and sufficient deformation capacity mainly through the tensile straining or yielding of the reinforcement steel.

Based on the load-to-deformation relationships, the ductility is usually measured using a ductility factor μ, which is the ratio between the ultimate deformation at failure to the elastic limit deformation. Considering the deterioration effects (e.g., reinforcement corrosion), the ductility factors of the structural constituents should be time-variant. The time-variant ductility factor at the component level, which is denoted as $\mu_c(t)$, can be expressed as

$$\mu_c(t) = \varphi_u(t) / \varphi_y(t) \tag{22}$$

where $\varphi_u(t)$ is the section curvature at the failure point and $\varphi_y(t)$ is the section curvature at the yielding point of the MCR curve, which can be obtained via sectional material nonlinear analysis. A larger ductility factor corresponds to a more ductile performance.

3.3 Time-variant redundancy of a structural system

For multi-girder bridges in which flexural failure is regarded as the main failure mode, the ductility of the components plays an important role in the ultimate load-carrying capacity of the system. Due to the direct influence on the plastic redistribution of the load for a bridge system, the ductility of a component significantly influences the capability of the system to continue to carry loads after the ductile failure of the most vulnerable component within the system [30]. This capability is referred to as the redundancy R_u and can be expressed by Eq. (23), which considers the time-variant effect [30, 31, 35, 40].

$$R_u(t) = \frac{LF_u(t)}{LF_e(t)} \tag{23}$$

where $LF_u(t)$ and $LF_e(t)$ are time-variant quantities that correspond to the deterioration effect.

In addition, to consider the time-variant effect, Eq. (4) and (8) can be reformulated as

$$N_u(t) = \frac{LF_u(t)}{L_{c0}} \tag{24}$$

$$N_e(t) = \frac{LF_e(t)}{L_{c0}} \tag{25}$$

where L_{c0} is the ultimate load-carrying capacity of single girder at the design state. Based on Eqs. (4), (8), (9), and (23), $R_u(t)$ can also be reformulated as

$$R_u(t) = \frac{LF_u(t)}{LF_e(t)} = \frac{LF_u(t)/L_{c0}}{LF_e(t)/L_{c0}} = \frac{N_u(t)}{N_e(t)} = \lambda(t) \tag{26}$$

$\lambda(t)$ is used to evaluate the plastic redistribution ability of the bridge system, which is the same as the original redundancy indicator R_u [31, 62]; hence, the redundancy R_u mainly reflects the plastic redistribution ability of the structural system. Therefore, for a multi-girder bridge system, when the topological configuration of the system is determined, the ductility of the component is the main factor that affects the redundancy.

According to Eq. (26), $1 < R_u \le R_{u,design}$, where $R_{u,design}$ is the redundancy at the design state. With the deterioration of materials, the ductility of the components gradually decreases, and '1' represents that the structural system has lost the ability to redistribute an applied load. Ghosn *et al.* [31] suggested a minimum value of 1.3 for R_u to ensure a redundant superstructure system.

3.4 System-level reliability considering the time-variant load-carrying mechanism

As presented in Fig. 5, in addition to the reduction of the load-carrying component strength and structural redundancy, material deterioration will also cause performance degradation of the load-transferring component, which will lead to the change of the loading-carrying mechanism and failure model and will influence the bridge system reliability directly.

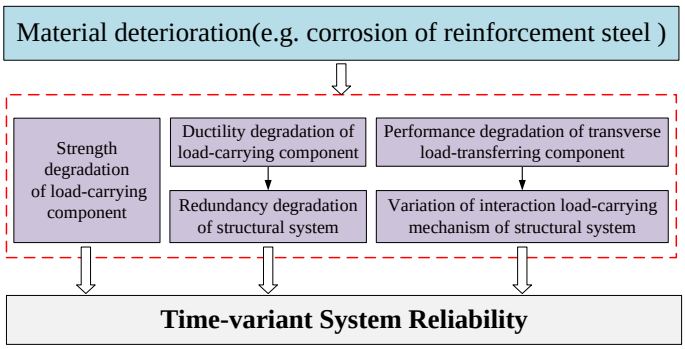

Fig. 5. Time-variant system reliability.

To consider the effect of the performance degradation of the load-transferring component on the change of the loading-carrying mechanism and failure model, a total probability formula is introduced to describe the failure probability of the bridge system P_S^f, which can be expressed as

$$\begin{aligned} P_S^f(t) &= \Pr\left\{R_S(t) < S_S(t)\Big|_{R_T(t)<S_T(t)}\right\}\cdot\Pr\left(R_T(t) < S_T(t)\right) + \\ &\quad \Pr\left\{R_S(t) < S_S(t)\Big|_{R_T(t)\geq S_T(t)}\right\}\cdot\Pr\left(R_T(t) \geq S_T(t)\right) \\ &= P_c^f(t)\cdot P_T^f(t) + P_{s,u}^f(t)\cdot(1\text{-}P_T^f(t)) \end{aligned} \tag{27}$$

where $P_T^f(t)$ is the failure probability of the transverse connection; $P_c^f(t)$ is the failure probability for SGFM; $P_{s,u}^f(t)$ is the failure probability for MGFM-PR; $R_T(t)$ and $S_T(t)$ are the resistance and effect, respectively, of the transverse connection; $R_S(t)$ and $S_S(t)$ are the resistance and effect, respectively, of the bridge system; and $\Pr\{\mathrm{E}\}$ is the probability of occurrence of event E.

The corresponding system reliability index $\beta_S(t)$ can be expressed as

$$\beta_S(t) = \text{-}\Phi^{-1}(P_S^f(t)) \tag{28}$$

The proposed assessment model reflects the effect of the stochastic variation of the interaction load-carrying mechanism on the bridge system reliability, which considers the effect of deterioration of the transverse connection on the structural interaction load-carrying mechanism. In addition to the overall reliability of the structural system, the efficiency indices PI_c and $PI_{s,u}$, which reflect the effects of different components on the system failure, are also critical for decision-making regarding bridge maintenance and reinforcement construction as they can determine the major cause of system failure initiation in a life-cycle context. Based on Bayes' theorem, two indices PI_c and $PI_{s,u}$ are defined to evaluate the probability contributions of SGFM and MGFM-PR to system failure.

$$PI_c = \frac{P_c^f \cdot P_T^f}{P_S^f} \tag{29}$$

$$PI_{s,u} = \frac{P_{s,u}^f \cdot (1\text{-}P_T^f)}{P_S^f} \tag{30}$$

4 Computational Procedure and Experimental Validation

The analytical procedure presented in this section consists of three modules: structural analysis of capacity and demand, probabilistic analysis, and reliability analysis modules. The probabilistic analysis module is developed for considering the uncertainties that are associated with the variables that are involved in the structural analysis module [47]. To account for time-variant effects (material deterioration), the analytical procedure is repeated for each time step during the investigated time interval. The six time steps are described below.

Step 1: Conduct sectional material nonlinear analysis as indicated in Fig. 6 to determine the moment resistance of component $R_c(t)$, which is equal to $M_u(t)$.

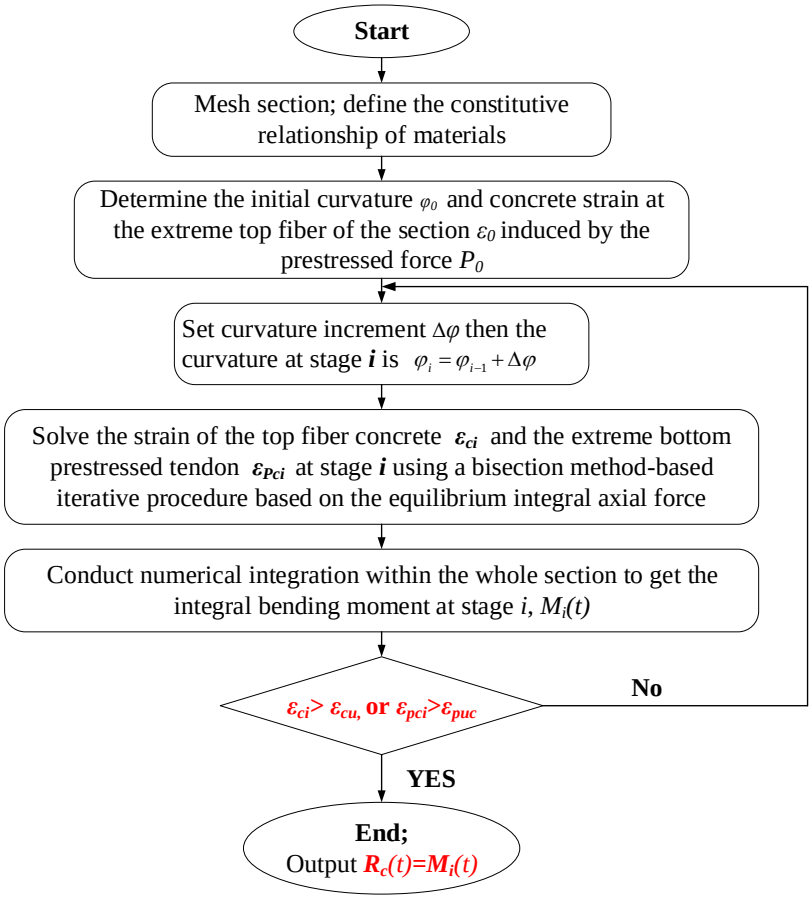

Fig. 6. Flowchart of numerical incremental algorithm for sectional MCR [40].

Step 2: Conduct the linear analytical procedure that is presented in Fig. 7 (a) to determine the ultimate vehicle load $L_c(t)$ for SGFM, the demands $S_c^G(t)$ and $S_c^V(t)$ in Eq. (2), the ultimate vehicle load $LF_e(t)$ for MGFM-ED, and the demands $S_s^G(t)$ and $S_{s,e}^V(t)$ in Eq. (6).

The Euler-Bernoulli beam element (Fig. 7 (b)) is used to establish the FEM for both single-girder and multi-girder bridges. The grillage model (Fig. 7 (c)) is used to simulate a multi-girder bridge system for MGFM-ED, which has been demonstrated to realize a satisfactory balance between accuracy and computational cost [63].

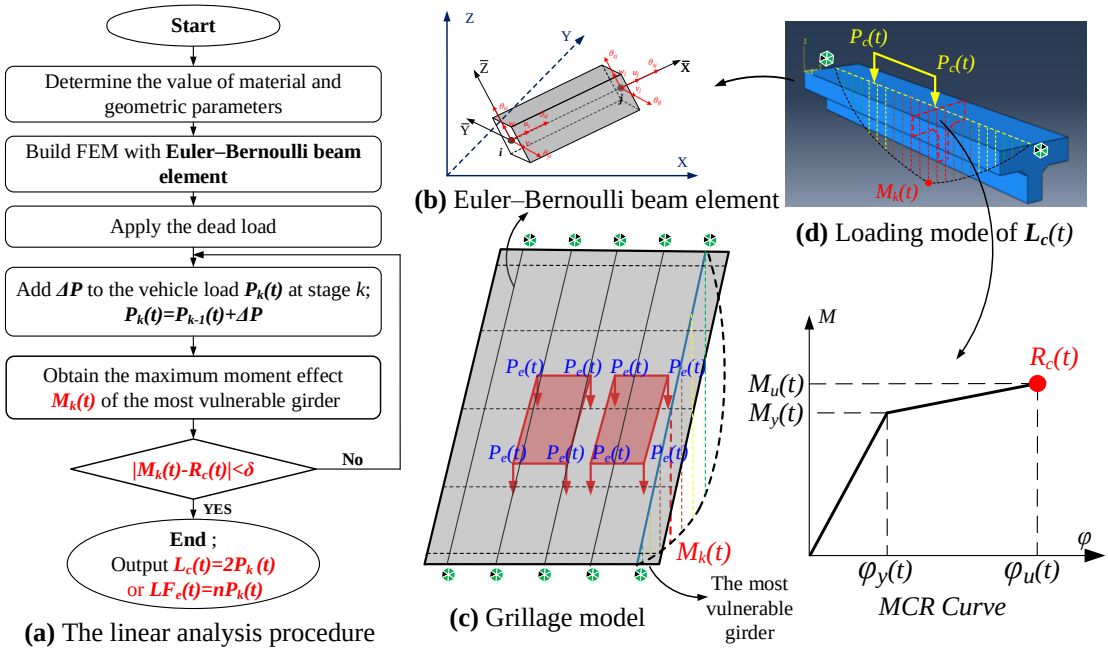

Fig. 7. Linear analytical procedure for SGFM and MGFM-ED.

Step 3: Destructive failure tests are field tests of in situ bridges in which each bridge is loaded until failure occurs, and they are utilized within this step. The main objective of destructive failure tests is to gain insight into the ultimate load-carrying capacities of bridges. According to a survey of destructive tests [23], most aging RC bridges are associated with reserve strength despite the presence of deterioration conditions, which may not be predicted by conventional analytical models. In this paper, a precise FEM is proposed, as presented in Fig. 8, which is evaluated on destructive failure test data and can be effectively applied to the failure analysis of in situ deteriorated multi-girder bridges.

The nonlinear analytical procedure for determining the ultimate vehicle load $LF_u(t)$ for MGFM-PR is presented in Fig. 8 (b), and the demands S_s^G and, $S_{s,u}^V$ are provided in Eq. (10). To calculate $LF_u(t)$, a grillage model with a fiber beam element is used to simulate the multi-girder system for MGFM-PR. As illustrated in Fig. 8 (c), the model is implemented with OpenSees [64]. The nonlinear beam column element (Fig. 8 (d)) is used to establish an FEM, in which five integration points are typically considered. The nonlinear characteristics in the cross-sections are captured by defining the uniaxial materials (unconfined concrete, confined concrete and reinforcement steel).

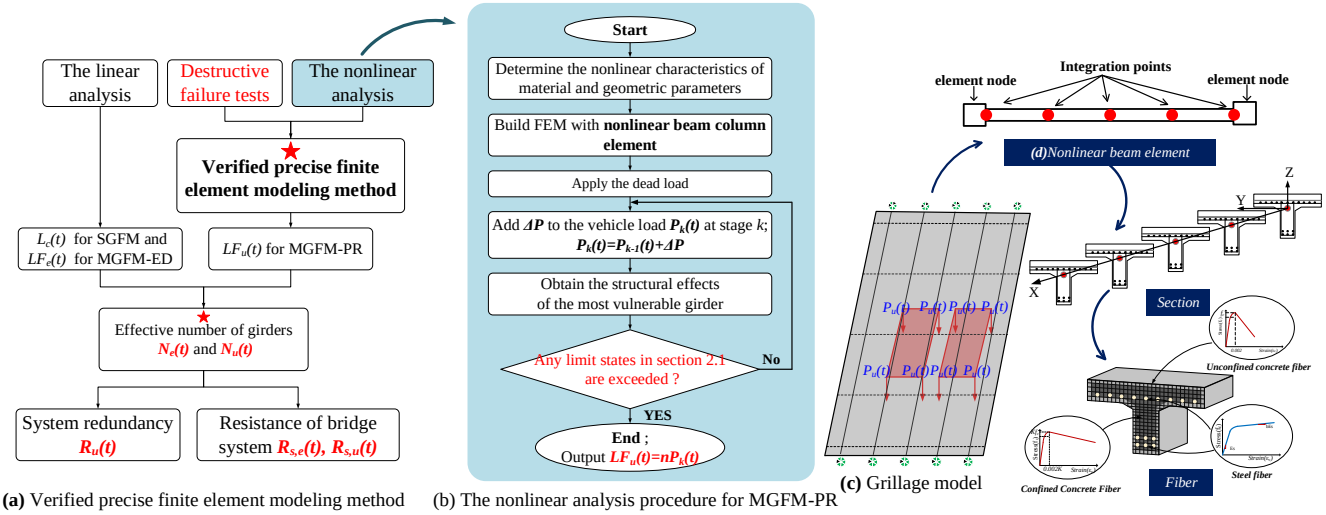

(a) Verified precise finite element modeling method (b) The nonlinear analysis procedure for MGFM-PR **(c)** Grillage model

Fig. 8. Finite element modeling for MGFM-PR

Step 4: In this step, the effective numbers of girders $N_e(t)$ and $N_u(t)$ and the system redundancy $R_u(t)$ are calculated using Eqs. (24), (25), and (26), as presented in Fig. 8 (a). To determine the load P, which is the necessary in the system reliability assessment, we should apply the load under the determined worst-case scenario of vehicle loading until the failure criterion is reached, as presented in Fig. 7 (a) and Fig. 8 (b). Then, $N_e(t)$ and $N_u(t)$ can be calculated as the ratios between loads, and $R_u(t)$ can be calculated as the ratio between $N_e(t)$ and $N_u(t)$.

Step 5: Conduct a reliability analysis with the limit state functions (31) to determine $P_T^f(t)$, $P_c^f(t)$, $P_{s,e}^f(t)$, and $P_{s,u}^f(t)$ in Eq. (27) using the first-order reliability method (FORM) [65, 66].

$$\begin{cases} Z_T(t) = R_T(t) - S_T^G(t) - S_T^V(t) \\ Z_c(t) = R_c(t) - S_c^G(t) - S_c^V(t) \\ Z_{s,e}(t) = R_{s,e}(t) - S_s^G(t) - S_{s,e}^V(t) \\ Z_{s,u}(t) = R_{s,u}(t) - S_s^G(t) - S_{s,u}^V(t) \end{cases} \tag{31}$$

where $Z_T(t)$, $R_T(t)$, $S_T^G(t)$, and $S_T^V(t)$ are the limit-state function, moment resistance, dead-load effects and vehicle-load effects, respectively, of the transverse connection. The corresponding reliability indices $\beta_T(t)$, $\beta_c(t)$, $\beta_{s,e}(t)$, and $\beta_{s,u}(t)$ can be calculated via Eq. (28).

Based on an accurate understanding of the failure modes of a single component and the bridge system, along with the whole-process structural behavior, a system reliability assessment is conducted from a global perspective. It follows from Eqs. (24), (25) and (26) that $R_{s,e}(t)$ and $R_{s,u}(t)$ in Eq. (31) can be computed as

$$R_{s,e}(t) = N_e(t) \cdot R_{c0} \tag{32}$$

$$R_{s,u}(t) = N_u(t) \cdot R_{c0} = R_u(t) \cdot N_e(t) \cdot R_{c0} \tag{33}$$

where R_{c0} is the moment resistance of a single girder at the design state. Moreover, $S_{s,e}^V$ and $S_{s,u}^V$ in Eq. (31) can be computed as $\sum M_i^v$, where M_i^v is the vehicle load effect of each girder for MGFM-ED and MGFM-PR, respectively, under the determined worst-case scenario of vehicle loading, as presented in Fig. 3. In this paper, a novel indicator, namely, the effective number of girders ($N_e(t)$, $N_u(t)$), is proposed for calculating the global load-carrying capacity of the structural system quantitatively, which avoids the shortcomings of the previously discussed series parallel method at the system level.

Step 6: Determine the failure probability P_S^f and reliability index β_S of the bridge system via Eq. (27) and (28), respectively, and compute PI_c and $PI_{s,u}$ via Eq. (29) and (30), respectively.

5 Illustrative Examples

5.1 Destructive failure test of investigated bridges

The first investigated bridge (IB1) is a cast-in-place, 9.2m simply supported RC T-girder bridge. Fig. 9 (a) and (b) present the dimensions of the bridge with the reinforcement layout. Based on standard tests that were conducted on cores and a reinforcing bar from the bridge, the basic material properties of the bridge were determined. The average values of the measured initial elastic modulus of concrete and the compressive strength were 23,530 and 23.5 MPa, respectively, and the yield stress of the reinforcement bar was 254.8 MPa. To explore the ultimate load-carrying capacity of IB1, Song *et al*. [67] conducted an in situ full-scale destructive test on the bridge. To simulate the actual vehicle loading, cyclic loading was imposed eccentrically, as illustrated in Fig. 9 (a), and the bridge was loaded to failure. The test span was instrumented such that measurements could be conducted to assess both the global and local responses of the bridge. Measurements were conducted at locations where a maximum response was expected. Fig. 9 (c) illustrates the test setup for IB1 in detail.

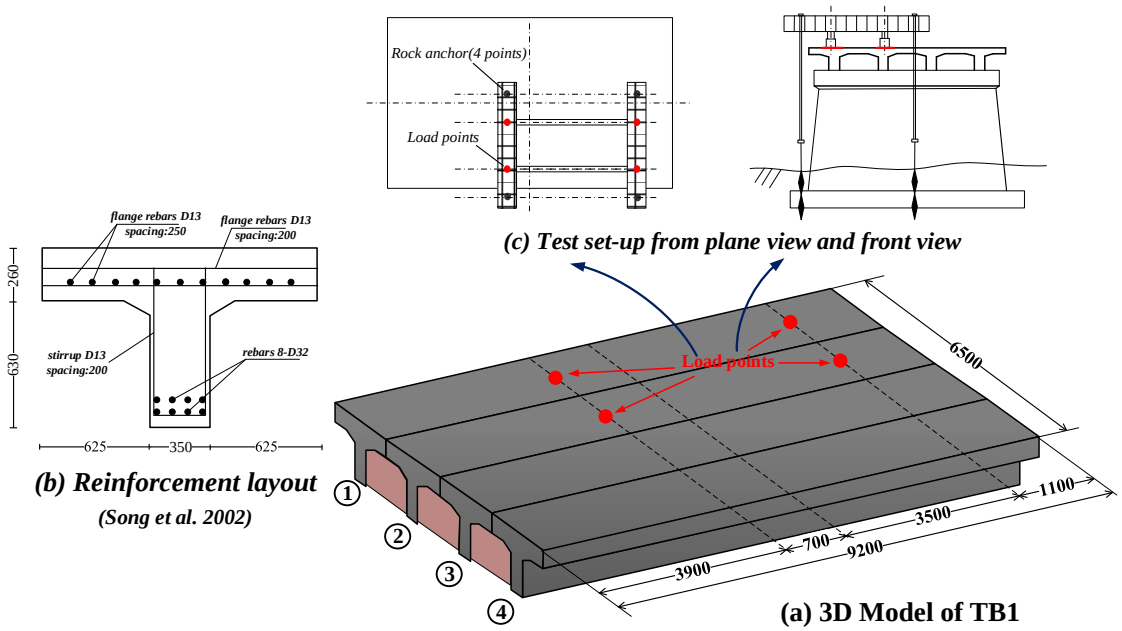

Fig. 9. Destructive failure test of IB1 (unit: mm).

The second investigated bridge (IB2) is a 20m simply supported PRC T-girder bridge that is composed of 6 T-girders, with 5 diaphragms, namely, two end diaphragms and three middle

diaphragms, distributed along the span uniformly. Fig. 10 (a) and (b) indicate the dimensions of the bridge and girder section. All T-girders were prefabricated with C50 concrete. The prestressed reinforcement was tensioned with a 1,600-MPa high-strength steel wire cone anchor jack, and the tension stress was controlled to 1,200 MPa. To explore the ultimate load-carrying capacity of IB2, Zhang [68] conducted an in situ full-scale destructive test of the bridge, as shown in Fig. 10 (c). Considering the tremendous loading amount in the destructive failure test of in situ bridge, the steel loading scheme was adopted. Fig. 10 (d) presents the test setup for IB2.

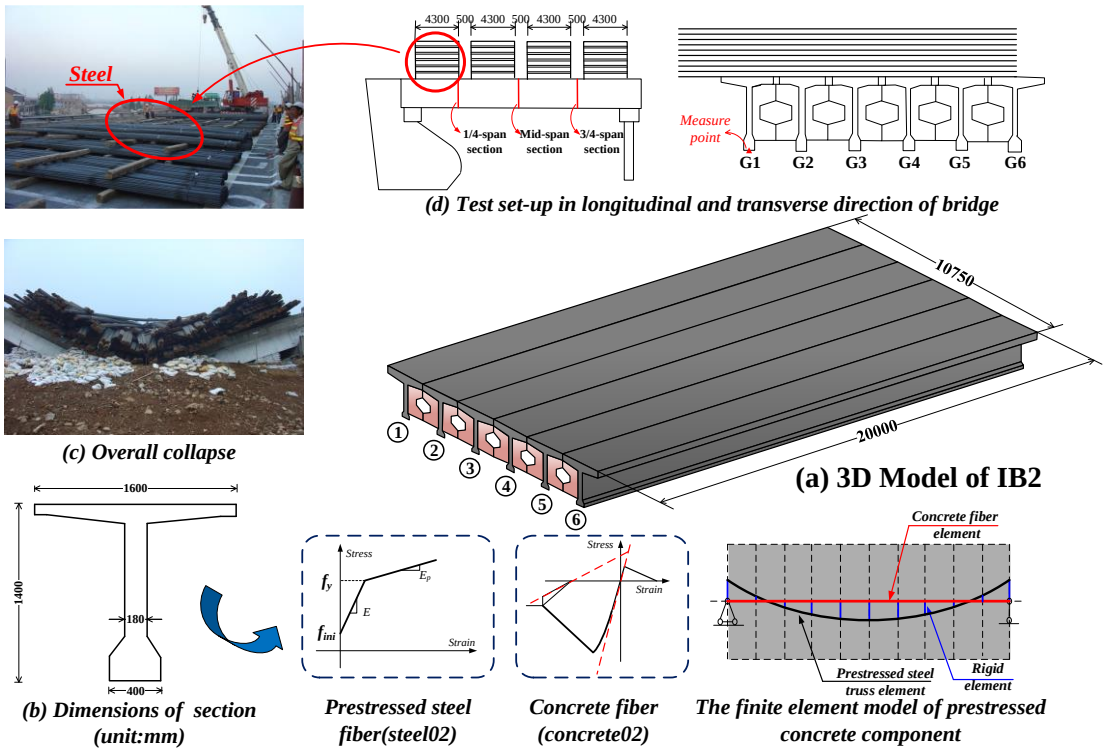

Fig. 10. Destructive failure test of IB2 (unit: mm).

5.2 Numerical model validation using destructive failure tests

The complete process of destructive failure is simulated in OpenSees using a fiber beam element to account for the nonlinear behavior. The analysis results, along with the test data and FEA results in references [67, 68], are presented in Fig. 11 and Fig. 12. Considering IB1 as an example, the results that were obtained in this paper for T-girders G1~ G3 accord well with test data, as shown in Fig. 11. For T-girder G4, the simulation results are more similar to the test data than the FEA results in the reference. For IB2, the analysis results for T-girder G1 are presented in Fig. 12 and are compared with the test data.

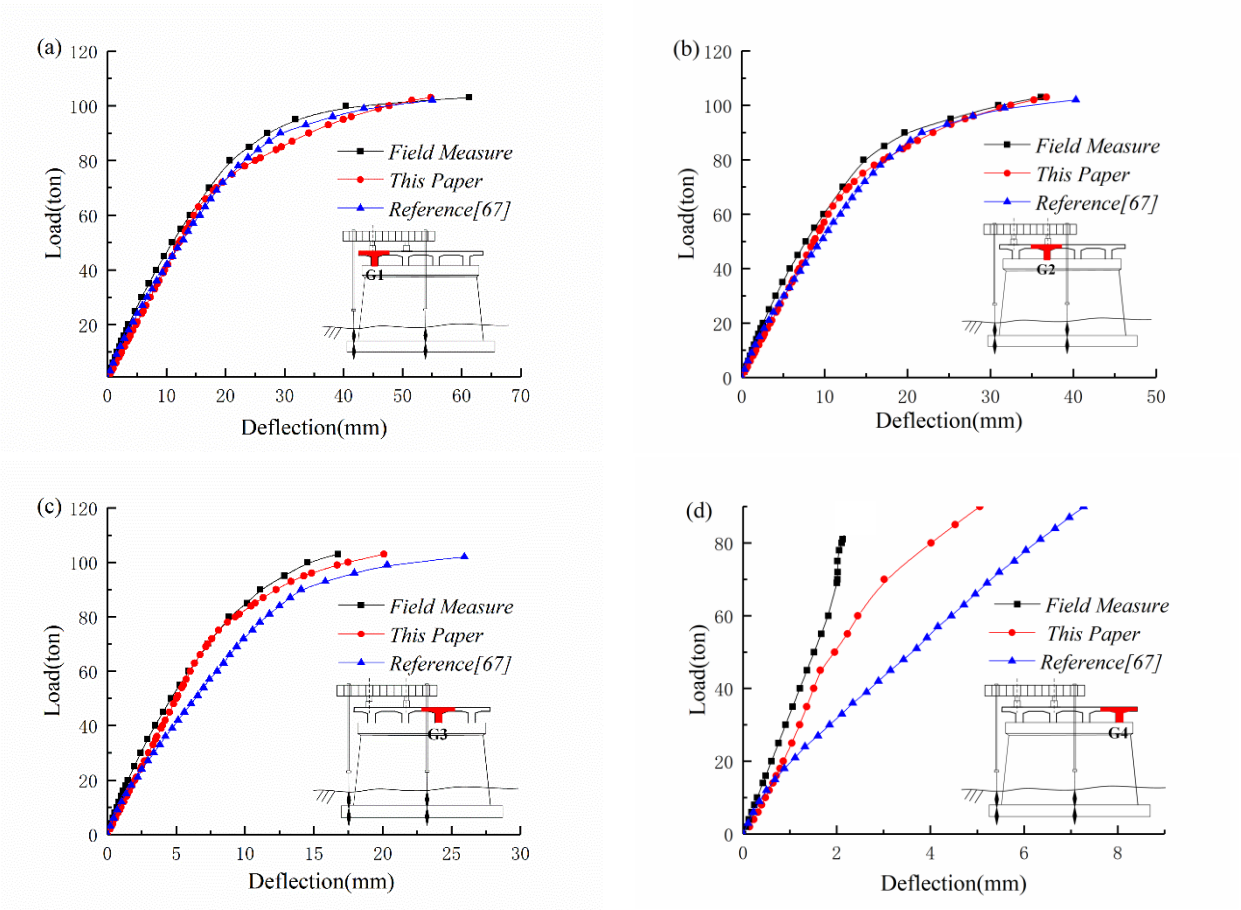

Fig. 11. Applied load versus deflection for IB1.

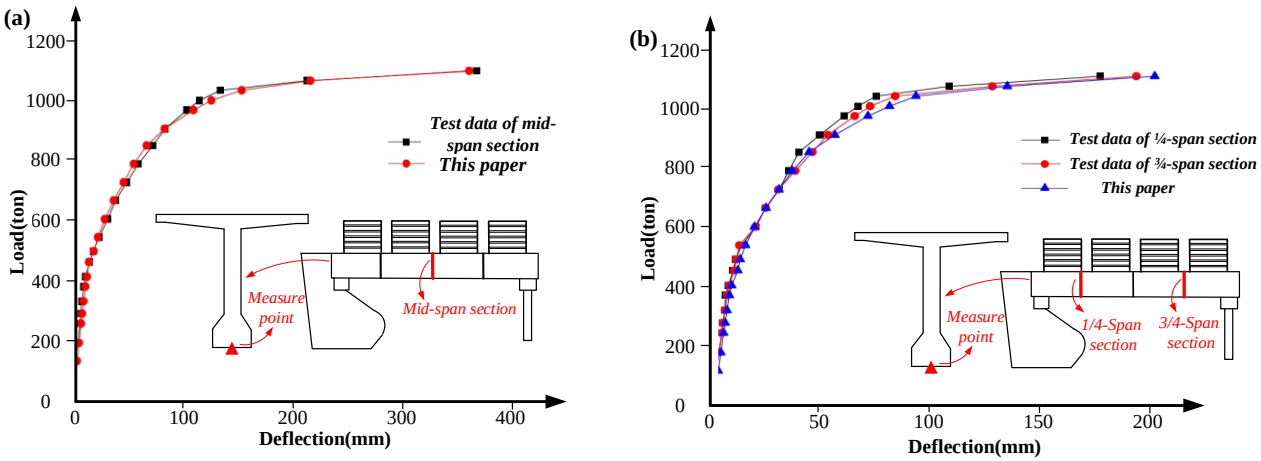

Fig. 12. Applied load versus deflection for IB2.

Thus, satisfactory accuracy of the proposed method for RC and PRC multi-girder bridges is demonstrated in the destructive failure tests. The time-variant structural performance in the worst-case scenario of vehicle loading is assessed in Sections 5.3-5.5.

5.3 Component-level performance analysis

The characteristic parameters of corroded reinforcement steel, such as f_{yc}, f_{uc} and f_{puc}, begin to decrease after the corrosion initiates, which would substantially affect the ductility and capacity of the component and the structure. To examine the effect of corrosion at the component level, $\varphi_y(t)$, $\varphi_u(t)$ and $\mu_c(t)$ as functions of the corrosion rate are presented in Fig. 13. $\varphi_u(t)$ decreases dramatically once the corrosion begins, whereas $\varphi_y(t)$ remains nearly constant for the investigated corrosion interval. The deteriorations of $\varphi_y(t)$ and $\varphi_u(t)$ result in a continuous reduction of the ductility $\mu_c(t)$. Considering IB1 as an example, $\mu_c(t)$ decreases from 10.4 to 3.7 for the interval of 0 to $\eta_{s,cr}$ since the yield plateau becomes dramatically shorter, as shown in Fig. 13 (a). Afterward, it increases gradually as $\varphi_y(t)$ and $\varphi_u(t)$ become closer after the disappearance of the yield plateau. For IB2, $\mu_c(t)$ decreases from 14.3 to 6.4 for the investigated corrosion interval, as presented in Fig. 13 (b). This is because the failure criterion of the section is gradually changed from the crushing of the top fiber-reinforced concrete to the tensile fracture of the prestressed tendons, and the latter is more easily satisfied [40].

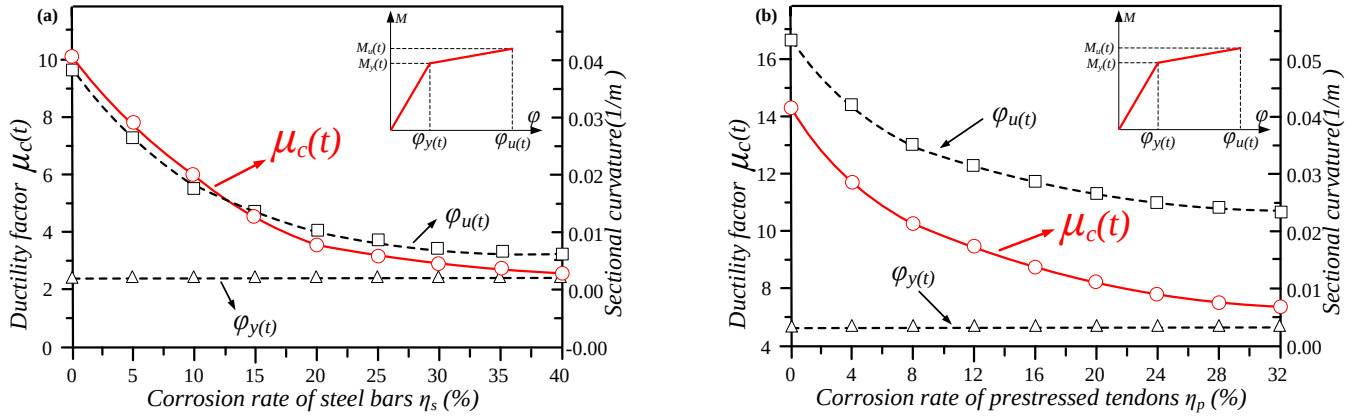

Fig. 13. Time-variant expected values of $\varphi_y(t)$, $\varphi_u(t)$, and $\mu_c(t)$ of (a) IB1 and (b) IB2.

5.4 System-level performance analysis

According to the analytical procedure in Section 4, the time-variant expected values of ultimate vehicle loads $LF_u(t)$, $LF_e(t)$ and $L_c(t)$ are presented in Fig. 14 (a) and Fig. 15. (a). The time-variant residual net area of reinforcement steel is computed based on the corrosion model [69, 70]. Considering IB1 as an example, the expected values of $LF_u(t)$, $LF_e(t)$ and $L_c(t)$ decrease after the corrosion begins at t = 20 years, as indicated in Fig. 14 (a). The trends of $LF_u(t)$ and $LF_e(t)$ are in agreement with that of $L_c(t)$, resulting in reductions of 23.5%, 16.9% and 19.8% at t = 100 years for $LF_u(t)$, $LF_e(t)$, and $L_c(t)$, respectively.

$LF_e(t)$ for MGFM-ED is always less than $LF_u(t)$ for MGFM-PR throughout the lifetime period, as shown in Fig. 14 (a) and Fig. 15. (a); hence, $LF_u(t)$ represents the ultimate load-carrying capacity of multi-girder bridges, which considers both the elastic distribution and plastic redistribution for system-level performance assessment.

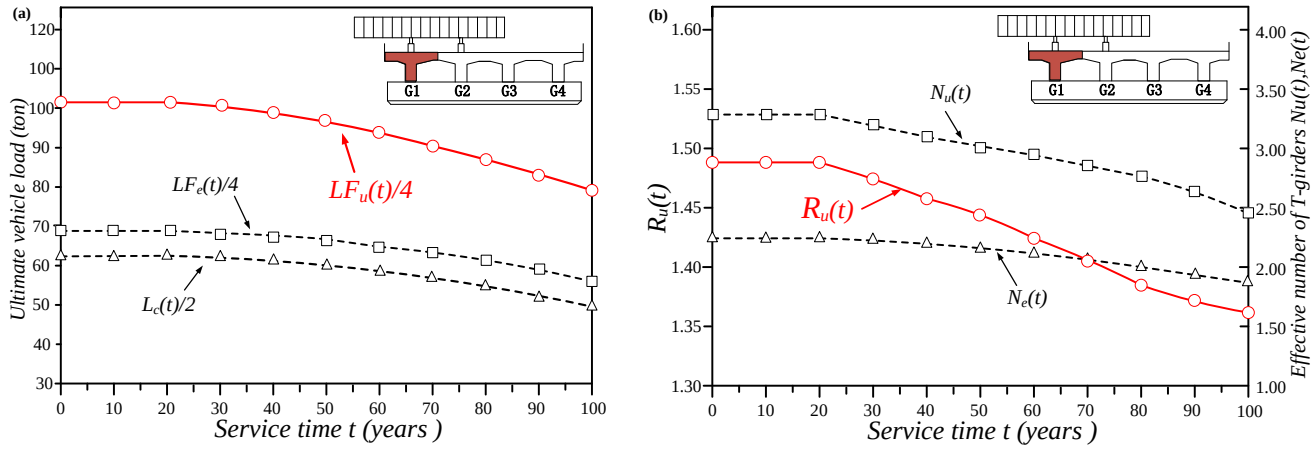

Fig. 14. Time-variant expected values of (a) the ultimate vehicle loads and (b) $N_u(t)$, $N_e(t)$ and $R_u(t)$ of IB1.

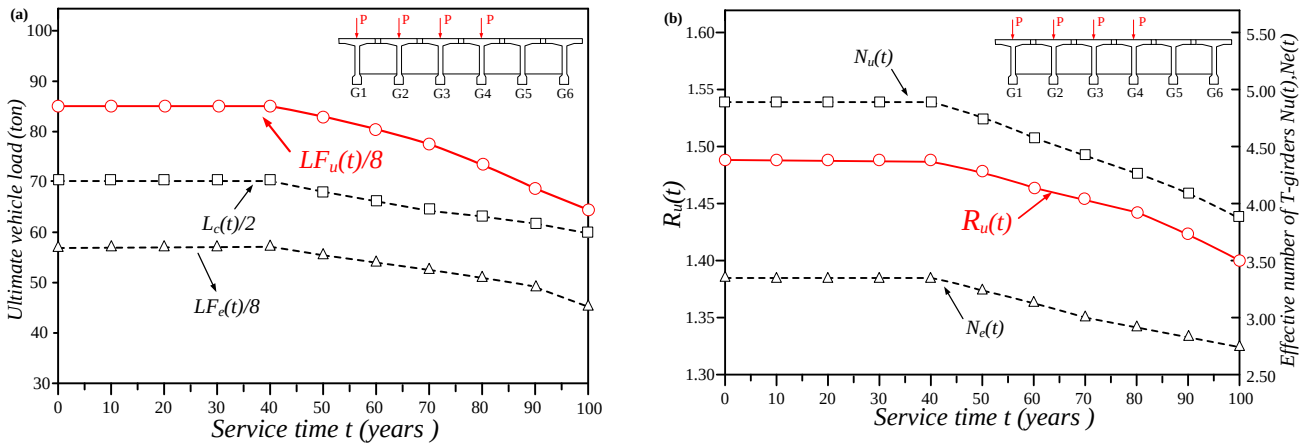

557 **Fig. 15**. Time-variant expected values of (a) the ultimate vehicle loads and (b) $N_u(t)$, $N_e(t)$ and $R_u(t)$ of IB2.

558

559 By using Eq. (24), (25), and (26), the expected values of the effective numbers of girders
560 $N_u(t)$, $N_e(t)$ and the redundancy $R_u(t)$ are shown in Fig. 14 (b) and Fig. 15. (b). Considering
561 IB1 at t = 20 years as an example for demonstrating the calculation in detail, the ultimate vehicle
562 load for SGFM is $L_{c0} = 2P_c = 2\times 63t$, the ultimate vehicle load for MGFM-ED is
563 $LF_e(t) = 4P_e = 4\times 68.63t$, and the ultimate vehicle load for MGFM-PR is
564 $LF_u(t) = 4P_u = 4\times 102t$. Thus, $N_u(t) = \frac{LF_u(t)}{L_{c0}} = \frac{4\times 102}{2\times 63} = 3.238$, $N_e(t) = \frac{LF_e(t)}{L_{c0}} = \frac{4\times 68.63}{2\times 63} = 2.179$,
565 and $R_u(t) = \frac{N_u(t)}{N_e(t)} = \frac{3.238}{2.179} = 1.486$. Based on the results, the bridge system can still continue to carry
566 48.6% of the load after the ductile failure of the most vulnerable component due to the effect of
567 plastic redistribution. The trends of $N_u(t)$ and $N_e(t)$ are in agreement with those of $LF_u(t)$ and $LF_e(t)$,
568 respectively. As indicated, the values of $N_u(t)$ and $N_e(t)$ at t = 100 years are approximately 76.5%
569 and 83.1%, respectively, of those at t = 20 years, while, $R_u(t)$ is larger than 1.30 throughout the
570 service life; hence, the redundancy is satisfactory.

571 Thus, $N_u(t)$ can explicitly quantify the vehicle-load distribution ability of a bridge system, as
572 presented in Fig. 14 (b) and Fig. 15 (b). By dividing $N_u(t)$ by $N_e(t)$ (which yields the redundancy
573 $R_u(t)$), the plastic redistribution ability of a bridge system is quantified.

5.5 Time-variant system reliability assessment

According to the analytical procedure in Section 4, the time-variant system reliability is calculated. As shown in Fig. 16, due to the effect of the elastic distribution of the transverse connection, the reliability index for MGFM-ED $\beta_{s,e}(t)$, is much larger than the reliability index for SGFM $\beta_c(t)$. The reliability index for MGFM-PR $\beta_{s,u}(t)$, is larger than $\beta_{s,e}(t)$, which reflects the effect of plastic redistribution on the capacity of the bridge system. According to the framework proposed in Section 3.4, the system reliability $\beta_S(t)$ is very close to $\beta_{s,u}(t)$ when the transverse connection does not deteriorate. However, it gradually becomes consistent with $\beta_c(t)$ with the deterioration of the transverse connection; hence, the time-variant load-carrying mechanism affects the reliability of the bridge system.

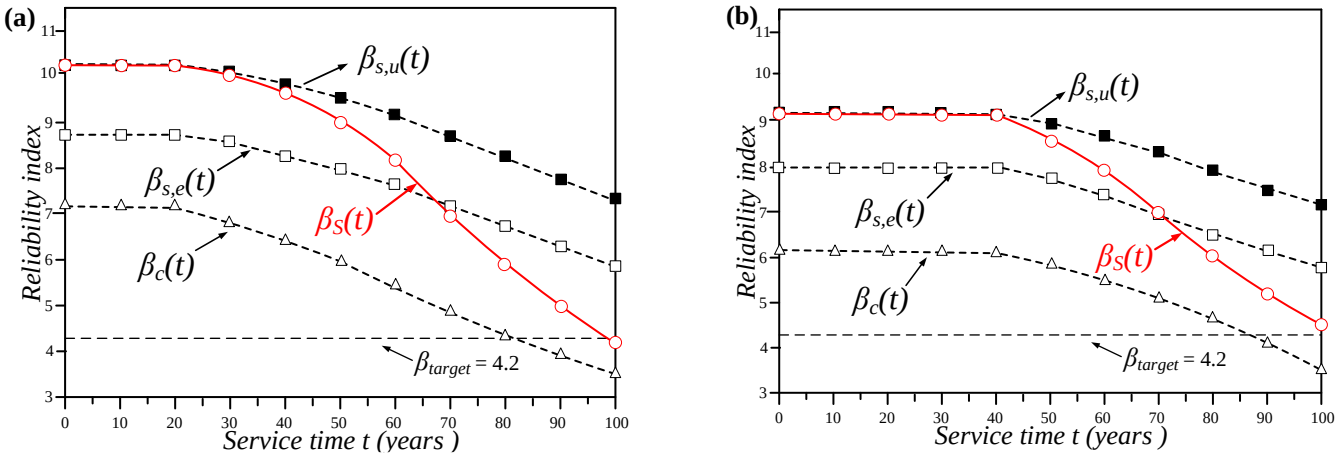

Fig. 16. Time-variant reliability of (a) IB1 and (b) IB2.

To further evaluate the effect of the variation of the load-carrying mechanism on the structural capability, the effect of the performance of the transverse connection on the system reliability at t = 40 years of IB1 is investigated. As shown in Fig. 17 (a), MGFM-ED and MGFM-PR consider only the effect of deterioration of the girder on the system capability and not the effect of deterioration of the transverse connection. In contrast, the proposed framework considers the effect of deterioration of the transverse connection on the variation of the load-carrying mechanism. When considering the deterioration of the transverse connection, the structural load-carrying mechanism gradually changes from MGFM to SGFM.

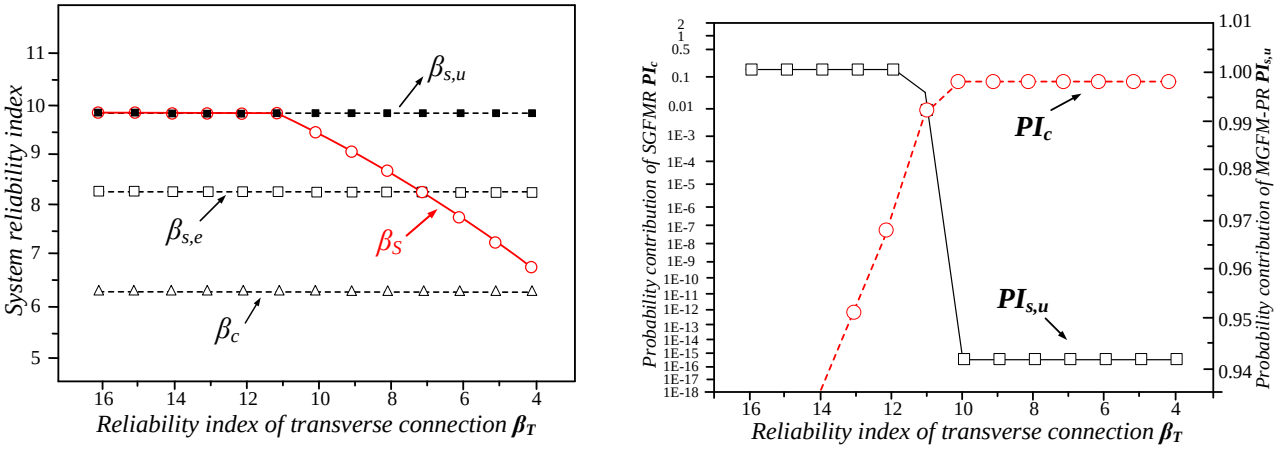

Fig. 17. (a) Expected values of β_S, $\beta_{s,u}$, $\beta_{s,e}$, and β_c; and (b) PI_c and $PI_{s,u}$.

As shown in Fig. 17 (b), the corresponding probability contributions of SGFM and MGFM-PR to the system failure are calculated via Eq. (29) and (30). The larger the reliability index of the transverse connection, the larger the probability contribution of MGFM-PR. For this scenario, increasing the performance of the girder is more effective. For a larger value of PI_c, it indicates that the transverse connection is associated with a poor condition. Special attention should be paid to performance assessment and management of transverse connection within the investigated bridge.

6 Conclusions

A novel approach is developed for evaluating the system reliability of multi-girder bridges, which considers the effects of the time-variant load-carrying mechanism and redundancy of the bridge system. The following conclusions are drawn:

1. Based on the investigative reports of actual accidents and full-scale destructive failure tests, three typical flexural failure modes for multi-girder bridges are assessed: SGFM, MGFM-ED and MGFM-PR. It is found that the performance of the transverse connection directly influences the flexural failure modes of the bridge system.
2. For quantitatively evaluating the elastic distribution and plastic redistribution of a vehicle load among multiple girders, a new indicator is proposed, namely, the effective number of girders. This indicator is used to calculate the global load-carrying system capacity in the system reliability assessment.

3. Through analyzing the time-variant behavior of the material, its deterioration leads to not only the reduction of the girder's resistance but also the deterioration of the girder's ductility, which further affects the plastic redistribution of the vehicle load at the system level. Hence, in addition to the time-variant structural component resistance, the time-variant redundancy of bridge system is an important factor that should be considered in the structural performance analysis process.
4. By considering the effect of deterioration of the transverse connection on the structural interaction load-carrying mechanism, a new reliability assessment framework for bridge systems is proposed.
5. An analytical procedure with detailed modeling techniques is established for implementing the proposed assessment framework. In this procedure, a sectional material nonlinear analysis for MCRs is conducted to capture the time-variant resistance and ductility of components. An incremental nonlinear finite element analysis of a fiber beam element using OpenSees is used to simulate the plastic redistribution of an applied load.
6. Full-scale destructive tests of two in situ deteriorated bridges are selected for evaluating the accuracy and feasibility of the proposed analytical procedure: a reinforced concrete (RC) T-girder bridge and a prestressed reinforced concrete (PRC) T-girder bridge. The results of the proposed simulation analytical procedure are in good agreement with the test data.
7. The feasibility and satisfactory performance of the proposed framework and procedure are evaluated using the RC and PRC T-girder bridges. The results demonstrate that the time-variant load-carrying mechanism and redundancy significantly affect the structural ultimate load-carrying capacity and reliability of deteriorated structures.

Nowadays, the bridges and infrastructural networks in many countries are facing the progressive deterioration of performance and safety issues. The results of this study could aid the design and management of more redundant structures in a life-cycle context. This goal can be achieved by proposing a method to reward adequately redundant designs by permitting less conservative member designs than is allowed by current design standard. Furthermore, more

644 studies should be conducted on the effects of spatial variability of the material corrosion on the
645 system performance (e.g., reliability, redundancy).

646 **Acknowledgments**

647 This work is supported by the Natural Science Foundation of Shaanxi Province, China [Grant No.
648 2020JM-219], the China Postdoctoral Science Foundation [Grant No. 2019M653519], and
649 Research Grants Council of the Hong Kong Special Administrative Region, China [Grant No.
650 PolyU 15219819].
651

References

[1] Frangopol DM. Life-cycle performance, management, and optimisation of structural systems under uncertainty: Accomplishments and challenges. Structure & Infrastructure Engineering. 2011;7:p.389-413.

[2] Frangopol DM, and Kim, S. Life-cycle of structures under uncertainty: emphasis on fatigue-sensitive civil and marine structures: CRC Press, Boca Raton; 2019.

[3] Frangopol DM, Dong Y, Sabatino S. Bridge life-cycle performance and cost: analysis, prediction, optimisation and decision-making. Structure and Infrastructure Engineering. 2017;13:1239-57.

[4] Akiyama M, Frangopol DM, Takenaka K. Reliability-based durability design and service life assessment of reinforced concrete deck slab of jetty structures. Structure and Infrastructure Engineering. 2017;13:468-77.

[5] Guo H, Dong Y, Gu X. Durability assessment of reinforced concrete structures considering global warming: A performance-based engineering and experimental approach. Construction and Building Materials. 2020;233:117251.

[6] Li Y, Dong Y, Frangopol DM, Gautam D. Long-term resilience and loss assessment of highway bridges under multiple natural hazards. Structure and Infrastructure Engineering. 2020;16:626-41.

[7] Hao S. I-35W bridge collapse. Journal of Bridge Engineering. 2010;15:608-14.

[8] Stark TD, Benekohal R, Fahnestock LA, Lafave JM, He J, Wittenkeller C. I-5 Skagit River Bridge Collapse Review. Journal of Performance of Constructed Facilities. 2016:04016061.

[9] Calvi GM, Moratti M, O'Reilly GJ, Scattarreggia N, Monteiro R, Malomo D et al. Once upon a Time in Italy: The Tale of the Morandi Bridge. Structural Engineering International. 2019;29:198-217.

[10] Morgese M, Ansari F, Domaneschi M, Cimellaro GP. Post-collapse analysis of Morandi's Polcevera viaduct in Genoa Italy. Journal of Civil Structural Health Monitoring. 2020;10:69-85.

[11] Zhu B, Frangopol DM. Effects of post-failure material behaviour on redundancy factor for design of structural components in nondeterministic systems. Structure and Infrastructure Engineering. 2015;11:466-85.

[12] Wang Z, Jin W, Dong Y, Frangopol DM. Hierarchical life-cycle design of reinforced concrete structures incorporating durability, economic efficiency and green objectives. Engineering Structures. 2018;157:119-31.

[13] Melchers RE. Assessment of existing structures—approaches and research needs. Journal of Structural Engineering-asce. 2001;127:406-11.

[14] Val DV, Trapper P. Probabilistic evaluation of initiation time of chloride-induced corrosion. Reliability Engineering & System Safety. 2008;93:364-72.

[15] Hamdia KM, Arafa M, Alqedra MA. Structural damage assessment criteria for reinforced concrete buildings by using a fuzzy analytic hierarchy process. Underground Space. 2018;3:243-9.

[16] Estes.AC, Frangopol DM. Repair optimization of highway bridges using system reliability approach. Journal of Structural Engineering. 1999.

[17] Li G. System reliability assessment of highway bridge structures: Institute of Geophysics, CSB; 2005.

[18] Akgül F, Frangopol DM. Lifetime performance analysis of existing steel girder bridge superstructures. Journal of Structural Engineering. 2004;130:1875-88.

695 [19] Akgül F, Frangopol DM. Lifetime performance analysis of existing reinforced concrete
696 bridges. I: Theory. Journal of Infrastructure Systems. 2005;11:122-8.
697 [20] Akgül F, Frangopol DM. Lifetime performance analysis of existing prestressed concrete bridge
698 superstructures. Journal of Structural Engineering. 2004;130:1889-903.
699 [21] Neves RA, Mohamedchateauneuf A, Venturini WS. Component and system reliability analysis
700 of nonlinear reinforced concrete grids with multiple failure modes. Structural Safety. 2008;30:183-
701 99.
702 [22] Neves RA, Chateauneuf A, Venturini WS, Lemaire M. Reliability analysis of reinforced
703 concrete grids with nonlinear material behavior. Reliability Engineering & System Safety.
704 2006;91:735-44.
705 [23] Ho IK, Shahrooz BM. Finite element modeling of a deteriorated R.C. slab bridge: lessons
706 learned and recommendations. Structural Engineering & Mechanics. 1998;6.
707 [24] Frangopol DM, Curley JP. Effects of damage and redundancy on structural reliability. Journal
708 of Structural Engineering. 1987;113:1533-49.
709 [25] Fu G, Frangopol DM. Balancing weight, system reliability and redundancy in a multiobjective
710 optimization framework. Structural Safety. 1990;7:165-75.
711 [26] Frangopol DM, R. N. Redundancy in highway bridges. Engineering Journal. 1991:Discussion
712 Paper 115.
713 [27] Frangopol DM, Iizuka M, Yoshida K. Redundancy measures for design and evaluation of
714 structural systems. Journal of Offshore Mechanics & Arctic Engineering, ASME. 1992;114:285-
715 90.
716 [28] Hendawi S, Frangopol DM. System reliability and redundancy in structural design and
717 evaluation. Structural Safety. 1994;16:47-71.
718 [29] Okasha NM, Frangopol DM. Lifetime-oriented multi-objective optimization of structural
719 maintenance considering system reliability, redundancy and life-cycle cost using GA. Structural
720 Safety. 2009;31:460-74.
721 [30] Okasha NM, Frangopol DM. Time-variant redundancy of structural systems. Structure &
722 Infrastructure Engineering. 2010;6:279-301.
723 [31] Ghosn M, Moses F, Frangopol DM. Redundancy and robustness of highway bridge
724 superstructures and substructures. Structure and Infrastructure Engineering. 2010;6:257-78.
725 [32] Zhu B, Frangopol DM. Reliability, redundancy and risk as performance indicators of structural
726 systems during their life-cycle. Engineering Structures. 2012;41:34-49.
727 [33] Zhu B, Frangopol DM. Effects of post-failure material behaviour on redundancy factor for
728 design of structural components in nondeterministic systems. Structure & Infrastructure
729 Engineering. 2015;11:466-85.
730 [34] Okasha NM, Frangopol DM. Redundancy of structural systems with and without maintenance:
731 An approach based on lifetime functions. Reliability Engineering & System Safety. 2017;95:520-
732 33.
733 [35] Saydam D, Frangopol DM. Time-dependent performance indicators of damaged bridge
734 superstructures. Engineering Structures. 2011;33:2458-71.
735 [36] Zhu B, Frangopol DM. Incorporation of structural health monitoring data on load effects in
736 the reliability and redundancy assessment of ship cross-sections using Bayesian updating.
737 Structural Health Monitoring. 2013;12:377-92.
738 [37] Wen YK, Song S. Structural reliability/redundancy under earthquakes. Journal of Structural

739 Engineering. 2004;129:56-67.
740 [38] Kim J, Williamson EB. Finite-element modeling of twin steel box-girder bridges for
741 redundancy evaluation. Journal of Bridge Engineering. 2015;20:4014106.
742 [39] Biondini F, Frangopol DM. Time-variant redundancy and failure times of deteriorating
743 concrete structures considering multiple limit states. Structure and Infrastructure Engineering.
744 2017;13:94-106.
745 [40] Tu B, Dong Y, Fang Z. Time-dependent reliability and redundancy of corroded prestressed
746 concrete bridges at material, component, and system levels. Journal of Bridge Engineering.
747 2019;24:04019085.
748 [41] Eamon CD, Nowak AS. Effects of edge-stiffening elements and diaphragms on bridge
749 resistance and load distribution. Journal of Bridge Engineering. 2002;7:258-66.
750 [42] Eamon CD, Nowak AS. Effect of secondary elements on bridge structural system reliability
751 considering moment capacity. Structural Safety. 2004;26:29-47.
752 [43] Kozy B, Tunstall S. Stability analysis and bracing for system buckling in twin I-girder bridges.
753 Bridge Structures. 2007;3:149-63.
754 [44] Razaqpur AG, Shedid MT, Nofal M. Inelastic load distribution in multi-girder composite
755 bridges. Engineering Structures. 2012;44:234-47.
756 [45] Kong S, Zhuang L, Tao M, Fan J. Load distribution factor for moment of composite bridges
757 with multi-box girders. Engineering Structures. 2020;215.
758 [46] China MoTotPsRo. Code for design of highway reinforced concrete and prestressed concrete
759 bridges and culverts.[In Chinese.] Beijing: People Communication Press; 2018.
760 [47] China MoTotPsRo. Unified standard for reliability design of highway engineering
761 structures[In Chinese.]. Beijing: People Communication Press; 2020.
762 [48] R H, Jan B, Casas J R ea. Guideline for inspection and condition assessment of existing
763 european railway bridges, SB-ICA, sustainable bridges: Including advices on the use of non-
764 destructive testing. 2007.
765 [49] Turan OT, Higgins C, Rosowsky DV. Statistical modeling of coupled shear-moment resistance
766 for rc bridge girders. Journal of Bridge Engineering. 2008;13:351-61.
767 [50] Tu B, Fang Z, Dong Y, Frangopol DM. Time-variant reliability analysis of widened
768 deteriorating prestressed concrete bridges considering shrinkage and creep. Engineering Structures.
769 2017;153:1-16.
770 [51] Zhang W, Shang D, Gu X. Stress-strain relationship of corroded steel bars. Journal of Tongji
771 University. 2006;34:586-92.
772 [52] Zhang W, Song X, Gu X, Li S. Tensile and fatigue behavior of corroded rebars. Construction
773 & Building Materials. 2012;34:409-17.
774 [53] Wang L, She Q, Zhang XH, Zhang JR. Study of mechanical property of prestressed strands
775 corroded in artificial climate. Journal of Highway & Transportation Research & Development.
776 2017.
777 [54] Nogueira CG, Leonel… ED. Probabilistic failure modelling of reinforced concrete structures
778 subjected to chloride penetration. International Journal of Advanced Structural Engineering. 2012;4.
779 [55] Liberati EAP, Nogueira CG, Leonel ED, Chateauneuf A. Nonlinear formulation based on FEM,
780 Mazars damage criterion and Fick's law applied to failure assessment of reinforced concrete
781 structures subjected to chloride ingress and reinforcements corrosion. Engineering Failure Analysis.
782 2014;46:247-68.

[56] Jianren Z, Yang L. Statistical models for the lifetime resistance of concrete bridges. Journal of Changsha University of science and Technology. 2004;01:27-33.
[57] Zhang M, Song H, Lim S, Akiyama M, Frangopol DM. Reliability estimation of corroded RC structures based on spatial variability using experimental evidence, probabilistic analysis and finite element method. Engineering Structures. 2019;192:30-52.
[58] A MZ, B NN, A MA, A SL, C KM. Effect of the correlation of steel corrosion in the transverse direction between tensile rebars on the structural performance of RC beams - ScienceDirect. Construction and Building Materials. 2020;264.
[59] Lim S, Akiyama M, Frangopol DM. Assessment of the structural performance of corrosion-affected RC members based on experimental study and probabilistic modeling. Engineering Structures. 2016;127:189-205.
[60] Lim S, Akiyama M, Frangopol DM, Jiang H. Experimental investigation of the spatial variability of the steel weight loss and corrosion cracking of reinforced concrete members: novel X-ray and digital image processing techniques. Structure & Infrastructure Engineering. 2016:118-34.
[61] Fajfar P. Equivalent ductility factors, taking into account low-cycle fatigue. Earthquake Engineering & Structural Dynamics. 1992;21:837-48.
[62] Ghosn M, Moses F. Redundancy in highway bridge superstructures. NCHRP Report. 1998.
[63] Hambly EC. Bridge deck behaviour: CRC Press; 1991.
[64] Mazzoni S, Mckenna F, Fenves GL. OpenSees Command Language Manual. 2001.
[65] Rackwitz R, Flessler B. Structural reliability under combined random load sequences. Computers & Structures. 1978;9:489-94.
[66] Wang X, Wu W, Liu Y, Ran Z. Surrogate-assisted two-phase tensioning strategy optimization for the system transformation process of a cable-stayed bridge. Engineering Optimization. 2020;52:603-19.
[67] Song H, You D, Byun K, Maekawa K. Finite element failure analysis of reinforced concrete T-girder bridges. Engineering Structures. 2002;24:151-62.
[68] Zhang J. Research on ultimate capacity of multi-beam concrete beam bridge: Southeast University; 2007.
[69] Enright MP, Frangopol DM. Probabilistic analysis of resistance degradation of reinforced concrete bridge beams under corrosion. Engineering Structures. 1998;20:960-71.
[70] Darmawan MS, Stewart MG. Spatial time-dependent reliability analysis of corroding pretensioned prestressed concrete bridge girders. Structural Safety. 2007;29:16-31.